Determination of bond lengths, atomic mean-square relative displacements, and local thermal expansion by means of soft-x-ray photoabsorption

L. Tröger, T. Yokoyama, D. Arvanitis, T. Lederer, M. Tischer, and K. Baberschke
Institut für Experimentalphysik, Freie Universität Berlin, Arnimallee 14, D-14195 Berlin, Germany
(Received 15 June 1993)

Temperature-dependent extended x-ray-absorption fine-structure (EXAFS) measurements at the oxygen and fluorine K edges of CuO, Cu_2O, ZnO, CaF_2, and LiF have been performed. We present an EXAFS analysis of bulk samples in the soft-x-ray region of $h\nu \leq 1500$ eV determining the moments of the radial pair distribution function (RDF) of the oxygen and fluorine nearest-neighbor bonds by use of the conventional cumulant expansion method, i.e., coordination numbers, bond lengths, atomic mean-square, and mean-cubic relative displacements of the RDF. It is shown that high-quality $K\alpha$-fluorescence-yield measurements, analyzed in combination with theoretical standards, allow a determination of nearest-neighbor distances within 0.015 Å and of coordination numbers with 10–20 % accuracy. Using quantum-mechanical models for the description of the atomic motions, the EXAFS Debye and Einstein temperatures, as well as the local thermal expansion of the bond under consideration, are obtained. In particular, these quantities for CaF_2 are found to be in good agreement with those measured by other techniques. In contrast to the fluorides, no thermal expansion could be observed up to room temperature for the transition-metal oxides, which confirms a recent finding of enhanced anharmonicity in the low-Z adsorbate-surface interaction. A detailed compilation is given of the majority of EXAFS studies from the literature where moments of the RDF higher than the second one are reported. For these compounds the local thermal expansion is quantum mechanically calculated in contrast to previous calculations that were performed in the classical limit. Debye temperatures and the local thermal expansion measured by EXAFS and other techniques agree well for fcc metals. For binary compounds like alkali halides or superionic conductors a deviation up to 100% can be found.

I. INTRODUCTION

Light elements like oxygen, nitrogen, and fluorine are major constituents of many inorganic materials. They also play an important role in catalytic reactions. Because of their small scattering cross sections, however, it is sometimes hard to probe them accurately by means of diffraction techniques. Extended x-ray-absorption fine-structure (EXAFS) spectroscopy is a tool to directly probe the local geometric and electronic environment of a *particular* atomic species of a sample on a short-range order scale.[1] The experimental setup of an EXAFS experiment in the soft x-ray region is, due to the high absorption cross section of the radiation, more sophisticated than for higher x-ray energies (heavier atoms): the experiment has to be performed in an ultrahigh vacuum (UHV) chamber and in almost all cases it is necessary to detect the absorption through secondary processes following the primary photoabsorption event.[2] The electron yield (EY) or photocurrent from the sample has been found to be proportional to the absorption coefficient of the sample[3–6] and is the easiest way to measure EXAFS spectra in the soft x-ray region.[7] This method has been widely used for the investigation of the local adsorption geometries and dynamics of low-Z adsorbates on metallic surfaces (surface EXAFS = SEXAFS).[2] However, following the early observation of the oscillatory structure above the oxygen K edge,[3] the quality of EXAFS spectra of light elements in *bulk materials* was limited by experimental problems arising from the highly structured transmission functions of the soft x-ray monochromators.[8] Consequently, soft x-ray data of bulk samples were mainly taken to serve as distance standards for SEXAFS studies[2]; no detailed quantitative EXAFS analysis or temperature-dependent study on *bulk samples* in this energy region ($h\nu \leq 1.5$ keV) meeting the high standards of the hard x-ray EXAFS analyses has been published so far. The detection of EXAFS through the secondary channel of the characteristic $K\alpha$ x-ray-fluorescence of the element of interest[9] together with the development of high-performance fluorescence detectors[10–13] had a considerable impact on the field of bulk EXAFS *in the soft x-ray region* within the past years: The much higher signal-to-background ratio of fluorescence yield (FY) detection in comparison to EY detection[10] facilitates the normalization of the experimental raw data and allows to overcome the problems arising from the structured transmission functions of soft x-ray monochromators mentioned above. Furthermore, the much larger information depth of FY detection in a non-grazing-incidence setup makes this technique a suitable tool to investigate the bulk properties of a sample.[14,15] Indeed, significant differences between FY and EY arising from the limited probing depth in EY were reported[14] questioning the quality of early oxygen EXAFS data taken in EY detection.[16] Following FY EXAFS studies at the oxygen and fluorine K edges of oxides, fluorides and high-T_c superconductors,[17–19] it was shown very recently that the

self-absorption effect which affects the experimentally measured FY EXAFS amplitude can be fully corrected and therefore a quantitative amplitude analysis of FY data is possible.[15,20] Furthermore, the transferability of the oxygen-metal EXAFS phase shift could be demonstrated, a long-standing problem, which allows an improved distance determination using soft x-ray EXAFS.[21] Single- and multiple-scattering *ab initio* XAFS calculations by means of the FEFF code[22–24] have been found to yield highly accurate theoretical standards also for EXAFS of light elements and allow to evaluate the importance of multiple-scattering contributions.[21]

Here we report a detailed analysis and comparison of temperature-dependent FY EXAFS measurements at the oxygen and fluorine K edges of metal oxides and fluorides. Based on the recent progress in soft FY EXAFS outlined above, we perform a state-of-the-art EXAFS analysis of bulk samples in the soft x-ray region of $h\nu \leq 1.5$ keV meeting the standards of EXAFS analyses in the harder x-ray region. Using theoretical standards obtained from the FEFF code we show that soft x-ray FY EXAFS measurements allow the determination of nearest-neighbor distances and coordination numbers within 0.015 Å and 10–20%, respectively. From the measured temperature variation of the Debye-Waller factors the Debye and Einstein temperatures of the nearest-neighbor bonds are obtained. It was shown that the local thermal expansion of a bond under consideration can be more accurately determined from the temperature dependence of the second and third moments of the RDF than through the linear term in the EXAFS phase.[25–27] Based on this finding we calculate the local thermal expansion in CaF_2 by use of a *quantum-mechanical* anharmonic oscillator model,[28–30] in good agreement with the one measured by other techniques. For the transition-metal oxides CuO, Cu_2O, and ZnO no thermal expansion could be observed between 30 and 300 K. This observation is discussed in combination to the large anharmonicity in the interaction of low-Z adsorbates on surfaces.[26] In order to compare our data to bulk EXAFS studies performed in the harder x-ray region, we recalculate the local thermal expansion for the majority of materials for which anharmonicity effects are quantitatively reported in the EXAFS literature[25–27,31–40] as all previous local thermal expansion calculations from EXAFS data were performed in the classical limit to the exception of Ref. 30.

The structure of the paper is as follows. Section II describes the experimental details, Secs. III and IV the theory of temperature-dependent EXAFS and the link to the determination of the local thermal expansion and the characteristic temperatures, respectively. In Secs. V and VI, the structural and dynamical analysis of the fluoride and oxide data is presented. A detailed comparison of the dynamical quantities to other bulk and surface systems is given in Sec. VII.

II. EXPERIMENT

The oxygen and fluorine FY EXAFS spectra were recorded at the storage ring BESSY using the plane-grating grazing-incidence monochromator SX-700II of the Freie Universität Berlin. An energy resolution of 1–3 eV was obtained at the O (532 eV) and F (690 eV) K edges, at a typical photon flux of $\approx 5\times 10^{10}$ photons/s. The measurements were carried out in an UHV chamber with a base pressure of $\leq 5\times 10^{-10}$ mbar. No bake-out to a temperature higher than 50 °C was performed. Up to 12 oxide and fluoride samples, including single crystals of Cu_2O, ZnO, CaF_2, LiF, and a pellet of CuO, were mounted on a copper sample holder attached to a commercial UHV manipulator. The copper oxide samples were previously characterized using photoemission measurements and were found to be of high purity.[41] A commercial liquid-nitrogen system was modified for operation with liquid helium. Temperatures down to 30 K were achieved at the sample. Temperature was monitored by two NiCr-Ni thermocouples attached to the sample holder. The samples were pressed mechanically against the holder, establishing a good thermal contact by means of a thin intermediate indium layer. The angle of x-ray incidence with respect to the sample surface could be varied. The characteristic x-ray fluorescence radiation was detected by means of a windowless Si(Li) detector[11,12,14] positioned along the electric field vector and operating with a peaking time of 3–8 μs. Also, total electron yield (TEY) spectra were measured with a channeltron. The energy resolution of the FY detector, about 140 eV, allowed to electronically isolate the oxygen or fluorine $K\alpha$ fluorescence peak[14] and to minimize the background due to other fluorescence or scattered x-ray contributions. To achieve a good signal-to-noise ratio, up to 50 FY spectra were accumulated, each recorded with a typical count rate of 3000–10 000 counts/s over energy ranges of 500–1100 eV for O and 600–1200 eV for F EXAFS scans. High-quality EXAFS data can only be obtained if the FY raw data are accurately normalized to the primary photon flux. In the soft x-ray region the photon flux is a strongly varying function of the photon energy because of absorption processes occurring at the optical elements of the monochromator. We found that TEY spectra of freshly argon-sputtered silicon wafers yielded an excellent measure of the monochromator transmission function over the energy range of 400–1600 eV as silicon has no absorption edges in this energy range. These spectra were used to normalize the raw data for the photon flux. The normalization with clean silicon yields the same results as the one based on condensed krypton multilayers used earlier[14] and is easier to perform. Figures 1 and 2 show the normalized FY spectra of CuO and CaF_2, respectively, at low temperatures and at 300 K. The edge-jump ratios at the oxygen and the fluorine K edge are ≈ 6 and ≈ 25, respectively. The oxygen EXAFS edge-jump ratio was limited by the transmission of second-order light through the monochromator. Due to the smaller atomic number of Ca with respect to Cu, the EXAFS amplitude decreases in Fig. 2 much more rapidly with increasing photon energy than in Fig. 1. Also, the damping of the EXAFS amplitude with increasing temperature can be seen by eye inspection for CaF_2 in contrast to the case of CuO. The experimentally measured FY EXAFS spectra still include self-absorption effects and were corrected in k space using a standard correction procedure to obtain the

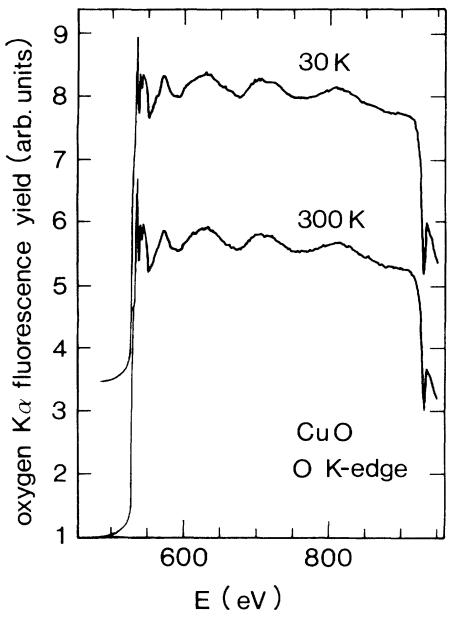

FIG. 1. Normalized fluorescence yield spectra at the oxygen K edge of CuO at 30 and 300 K. Warm and cold spectra are vertically shifted against each other.

correct EXAFS.[15] For the LiF and CaF_2 samples, the self-absorption effect was reduced to $\approx 25\%$ and $\approx 5\%$ of the EXAFS amplitude, respectively, by collecting the $K\alpha$ fluorescence at a 6° grazing angle with respect to the sample surface plane. This reduced the FY information depth to ≈ 3300 Å for LiF and 450 Å for CaF_2. The heavier transition-metal atoms weaken the effect of the self-absorption in the transition metal oxides compared to the LiF and CaF_2 data so that the $K\alpha$ fluorescence of the oxides was measured at a 30° grazing angle, yielding a self-absorption of $\approx 30\%$ and a FY information depth of ≈ 800 Å.

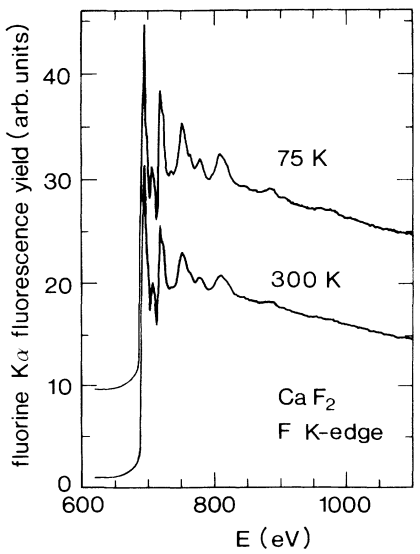

FIG. 2. Normalized fluorescence yield spectra at the fluorine K edge of CaF_2 at 75 and 300 K. Warm and cold spectra are vertically shifted against each other. The thermal damping of the CaF_2 EXAFS at room temperature is seen.

III. THE TEMPERATURE DEPENDENCE OF THE MOMENTS OF THE RADIAL PAIR DISTRIBUTION FUNCTION

In a solid exhibiting local static or dynamic disorder the positions of a single shell of atoms around a central atom have to be described in terms of the radial pair distribution function (RDF) $\rho(r)$. $\rho(r)dr$ is proportional to the probability of finding an atom of the shell under consideration in the distance range r to $r+dr$ around the central atom. We define $\int \rho(r)dr = N$, where N is the number of atoms of the shell. Since we are studying the temperature dependence of the local atomic environment in systems which exhibit anharmonic behavior, we formulate the EXAFS equation in terms of $\rho(T,r)$. The K shell EXAFS $k\chi(T,k)$ of a single-scattering contribution of a single shell of atoms in a cubic system can be written as[1]

$$k\chi(T,k) = S_0^2(k)F(k)\int \frac{\rho(T,r)}{r^2}\exp(-2r/\lambda) \times \sin[2kr+\varphi(k)]dr \ , \quad (1)$$

where k is the photoelectron wave number, $S_0^2(k)$ is an amplitude reduction factor due to many-body effects, $F(k)$ the backscattering amplitude, and $\varphi(k)$ the total EXAFS phase-shift of the atomic species of the shell. Although the mean free path λ of the photoelectron depends on the wave number k, in the following derivation it is chosen to be constant keeping in mind that this assumption may limit the accuracy in the analysis of some of the EXAFS parameters. Equation (1) states that EXAFS directly measures the Fourier transform of the *effective* RDF

$$\rho_{\text{eff}}(T,r) = \rho(T,r)\exp(-2r/\lambda)/r^2 \ .$$

However, we want to express the temperature-dependent EXAFS $k\chi(T,k)$ in terms of the moments of the *true* RDF $\rho(T,r)$ at the temperature T; in particular, the coordination number $N = \int \rho(T,r)dr$, the average distance between central and backscattering atom

$$R(T) \equiv \langle r \rangle_T = (1/N)\int r\rho(T,r)dr \ ,$$

the mean-square relative displacement (MSRD)

$$\sigma^2(T) \equiv \langle (r - R(T))^2 \rangle_T \ ,$$

and the mean-cubic relative displacement (MCRD)

$$c_3(T) \equiv \langle (r - R(T))^3 \rangle_T$$

at the temperature T. Neglecting higher moments and using the cumulant expansion,[34,42,43] Eq. (1) can be written as

$$k\chi(T,k) = A(T,k)\sin\phi(T,k) \ , \quad (2)$$

with

$$A(T,k)=\frac{S_0^2(k)F(k)}{R^2(T)}N\exp[-2R(T)/\lambda]\times\exp[-2\sigma^2(T)k^2] \quad (2a)$$

and

$$\phi(T,k)=2k\left[R(T)-\sigma^2(T)\left[\frac{2}{R(T)}+\frac{2}{\lambda}\right]\right]-\frac{4}{3}c_3(T)k^3+\varphi(k)\ . \quad (2b)$$

In noncubic systems, N has to be replaced by the effective coordination number N^* of the shell which depends on the orientation of the crystal with respect to the electric-field vector.[1] All our investigated samples except ZnO and CuO have cubic symmetry. Equation (2) can also be formulated in terms of the cumulants or moments of the *effective* RDF.[42] The term in square brackets in Eq. (2b) is the first moment of the effective RDF. The correction term

$$\sigma^2(T)[2/R(T)+2/\lambda]$$

arises from the fact that the EXAFS measurement overweights lower distances through the damping factor $R^{-2}\exp(-2R/\lambda)$ of the photoelectron. Higher moments of the true and effective RDF only differ by negligible terms of the order of σ^2/R^2. The EXAFS determined from the experiment is a sum of single-scattering contributions of the form (2) and multiple-scattering contributions of a more complicated form, including three- and many-body correlation functions. The EXAFS contribution of the first shell of atoms around the central absorbing atom of the form (2) is obtained from the measured total EXAFS $k\chi(T,k)$ by conventional Fourier-transform techniques, i.e., by transforming into r space, isolating the first shell by means of a window function, and inverse Fourier transforming into k space again.[1]

Absolute values of the parameters of interest N^*, $R(T)$, $\sigma^2(T)$, and $c_3(T)$ can be obtained by k fitting the experimentally measured first shell contribution using as input parameters for the fit the ones of experimental or theoretical standards.[44–46] We use here theoretical standards obtained by means of the FEFF code[22–24] (version 5.04) for our k-fitting analysis.

However, the *relative* variation of R, σ^2, and MCRD c_3 between two temperatures T_1 and T_2 can be determined with higher accuracy in a straightforward manner from the experimental data sets $k\chi(T_1,k)$ and $k\chi(T_2,k)$ by applying the ratio method[34,42,47]: Assuming the quantities $F(k)$, $\varphi(k)$, $S_0^2(k)$, and λ to be the same at T_1 and T_2, one obtains from Eq. (2) for the logarithmic EXAFS amplitude ratio and the linear phase difference between the temperatures T_2 and T_1 the expressions[48]

$$\ln\left[\frac{A(T_2,k)}{A(T_1,k)}\right]=-2\,\Delta\sigma^2(T_2,T_1)k^2 \quad (3a)$$

and

$$\frac{1}{k}[\phi(T_2,k)-\phi(T_1,k)]=2\left[\Delta R(T_2,T_1)-\Delta\sigma^2(T_2,T_1)\left[\frac{2}{R(T_1)}+\frac{2}{\lambda}\right]\right]-\frac{4}{3}\Delta c_3(T_2,T_1)k^2\ , \quad (3b)$$

where $\Delta\sigma^2(T_2,T_1)=\sigma^2(T_2)-\sigma^2(T_1)$, $\Delta c_3(T_2,T_1)=c_3(T_2)-c_3(T_1)$, and $\Delta R(T_2,T_1)=R(T_2)-R(T_1)$. Equations (3a) and (3b) yield $\Delta\sigma^2$ and Δc_3, the change in width and asymmetry of the true RDF, respectively, with respect to the reference temperature T_1. The intercept of the phase difference is discussed in the next section. In Sec. VI, we determine the temperature-dependent variation of σ^2 and c_3 in our experimental data sets using the ratio method outlined above. It was checked, however, that a k-fitting analysis of the experimental data measured at a temperature T_2 *using the experimental data at the temperature* T_1 *as a standard* yields identical results. Typically, there are only three free parameters in such a fit, i.e., the kinetic-energy reference of the photoelectron E_0 and N^* being fixed to the values at the temperature T_1. This number is much smaller than the number of independent parameters even for k ranges of $\Delta k\approx 9$ Å^{-1}. Under these circumstances anharmonicity effects (Δc_3) are quantitatively measurable, as was also shown recently.[26,36,49]

IV. LOCAL THERMAL EXPANSION, MEAN-SQUARE RELATIVE DISPLACEMENT AND CHARACTERISTIC TEMPERATURES

The linear thermal expansion $\Delta R(T_2,T_1)=R(T_2)-R(T_1)$ from the local view of EXAFS can be determined from the intercept of the $1/k$-weighted phase difference plot versus k^2; see Eq. (3b). However, this determination *through the linear term in the EXAFS phase* suffers from two basic limitations. First, a typical value of linear thermal expansion for a temperature difference of $T_2-T_1=300$ K is $\Delta R(T_2,T_1)=5\times10^{-3}$ Å. Thus a relative distance determination of better than 10^{-3} would be required which is in the limits of the accuracy of EXAFS. Second, the term

$$\Delta\sigma^2(T_2,T_1)[2/R(T_1)+2/\lambda]$$

has to be taken into account since it is of the same order as $\Delta R(T_2,T_1)$.[50] The k dependence of the mean free path λ of the photoelectron[1] and the experimental error of $\Delta\sigma^2(T_2,T_1)$ limits the precision with which it can be determined. However, in some cases, when very high-quality data can be measured or the experimental temperature interval is large, the local thermal expansion can be monitored through the linear term in the EXAFS phase.[37,40]

In the following an alternative, more precise method of determining the local thermal expansion from an EXAFS measurement is discussed, *relying only on the temperature dependence of* σ^2 *and* c_3 and first used in Refs. 25–27. It had been noticed that an asymmetric correction to a per-

fect Gaussian RDF induces a shift of the mean distance which is proportional to the asymmetry parameter.[51] This is also known in other spectroscopic techniques.[52] Linking this to the cumulant and moment expansion it was shown that for a moderately distorted Gaussian-type RDF with the moments $\sigma^2(T)$ and $c_3(T)$ the mean distance $R(T)$ can be written to first order as[26]

$$R(T)=r_0(T)+\frac{\sigma^3(T)}{2\sigma^2(T)} , \tag{4}$$

where $r_0(T)$ is the maximum of the RDF at the temperature T. In the classical limit, $r_0(T)$ is temperature independent and takes the minimum r_0 of the effective pair potential mediating the absorber-backscatterer interaction. Therefore, the local thermal expansion $R(T_2)-R(T_1)$ is

$$\Delta R(T_2,T_1)=\frac{\sigma^3(T_2)}{2\sigma^2(T_2)}-\frac{\sigma^3(T_1)}{2\sigma^2(T_1)} . \tag{5}$$

Under additional assumptions this expression was used by Wenzel and co-workers[25,26] to relate the local thermal expansion $\Delta R(T_2,T_1)$ to the measured values $\Delta\sigma^2(T_2,T_1)$ and $\Delta c_3(T_2,T_1)$, and the local thermal expansion was calculated for several bulk and surface systems. Yokoyama, Satsukawa, and Ohta[27] used model pair potentials of a Morse and a Madelung type to fit the experimentally observed temperature dependence of $\Delta\sigma^2$ and Δc_3 in several metals and metal bromides and obtained the RDF $\rho(T,r)$ in the classical limit from these potentials. From $\rho(T,r)$ the net local thermal expansion and the coefficient of the linear local thermal expansion were evaluated. It is interesting to note that Wenzel's and Yokoyama's approach is of advantage with respect to the measurement of the local thermal expansion through the linear term in the EXAFS phase because only the measured $\Delta\sigma^2(T_2,T_1)$ and $\Delta c_3(T_2,T_1)$ do enter the calculations. The relative error of the local thermal expansion is therefore of the order of the relative errors of $\Delta\sigma^2(T_2,T_1)$ and $\Delta c_3(T_2,T_1)$, typically around 10–20% even for systems where the thermal expansion cannot be measured through the linear term in the EXAFS phase.

The MSRD of the central absorbing and backscattering atom differs from the sum of mean-square displacements of these two atoms by the displacement correlation function.[53] In the harmonic approximation calculations of $\sigma^2(T)$ based on lattice-dynamical models have been performed for fcc metals[54] and adsorbates on metal surfaces,[55] but no exact calculations of $c_3(T)$ are known. Simplifying assumptions are (i) models of the Einstein-type, assuming uncorrelated atomic motions and replacing the phonon density of states (DOS) by a δ function at the Einstein frequency ω_E, and (ii) the *harmonic* Debye-model, assuming only acoustic phonons which yields a parabolic phonon DOS with a cutoff (=Debye) frequency, ω_D.[53] In a harmonic Einstein model, introducing the Einstein temperature $\Theta_E=\hbar\omega_E/k_B$, $\sigma^2(T)$ is given by[54]

$$\sigma^2(T)=\frac{\hbar^2}{2\mu k_B\Theta_E}\coth\left[\frac{\Theta_E}{2T}\right] , \tag{6}$$

where μ is the reduced mass of the atom pair. It should be noted that correlation effects can empirically be taken into account through a different ω_E (or Θ_E) for each bond. For fcc metals, the Einstein frequency ω_E for the nearest-neighbor bond was shown to be equal to the square root of the second moment of the phonon DOS.[56] Recently, $\sigma^2(T)$, $c_3(T)$, and the thermal expansion have been calculated in a quantum-mechanical Einstein model based on an *anharmonic* effective pair potential of the form

$$V(r-r_0)=\gamma/2(r-r_0)^2-\beta(r-r_0)^3+\cdots , \tag{7}$$

yielding Eq. (6) for $\sigma^2(T)$ and furthermore[28–30]

$$c_3(T)=\frac{\hbar^6\beta}{\mu^3k_B^4\Theta_E^4}\left[\frac{3}{2}\coth^2\left[\frac{\Theta_E}{2T}\right]-1\right] , \tag{8}$$

$$R(T)-r_0=\frac{3}{2}\frac{\hbar^4\beta}{\mu^2k_B^3\Theta_E^3}\coth\left[\frac{\Theta_E}{2T}\right] , \tag{9}$$

where r_0 is the minimum of the effective pair potential[57] and

$$\gamma=\mu\omega_E^2=\mu\hbar^{-2}k_B^2\Theta_E^2 . \tag{10}$$

This yields the coefficient

$$\alpha(T)=R(0\text{ K})^{-1}dR(T)/dT$$

of the local linear thermal expansion

$$\alpha(T)=\frac{3\hbar^4\beta}{R(0\text{ K})\mu^2k_B^3\Theta_E^4}\left[\frac{\Theta_E}{2T}\right]^2\sinh^{-2}\left[\frac{\Theta_E}{2T}\right] . \tag{11}$$

The coupled set of equations (6)–(11) contains only three temperature-independent parameters, γ or Θ_E, β, and r_0. The Einstein temperature Θ_E in this model is identical to the one in the harmonic approximation. $\sigma^2(T)$ only depends on γ or Θ_E, $c_3(T)$ only on β, and Θ_E. The *absolute* bond distance $R(0\text{ K})$ enters only in the coefficient $\alpha(T)$ of the local linear thermal expansion of Eq. (11). Consequently, from a *single* pair of the quantities $\Delta\sigma^2(T_2,T_1)$ and $\Delta c_3(T_2,T_1)$ in addition to the nearest-neighbor distance at low temperature $R(T_1)$, the full temperature dependence of all the previous parameters for the particular bond under consideration is obtained. In the high-temperature limit Eqs. (6)–(11) fulfill Eq. (4). In Sec. VI, we will determine the linear thermal expansion by use of Eq. (11). The approximation of the true crystal potential by the simple anharmonic Einstein model may be a possible source of errors; however, this method is more accurate than the measurement through the linear term in the EXAFS phase.

It is clear that the harmonic Debye model[53] cannot be used to estimate thermal expansion. But since anharmonicity is introduced as a weak anharmonic perturbation the temperature dependence of σ^2 in such systems can still be described by the Debye model which in the past has been applied successfully to fcc metals,[54,58] gold clusters[59] and also biatomic crystals.[60–62] It is derived for monoatomic, cubic systems, which may induce errors in applying it to biatomic samples. As the chief advan-

tage of the Debye model the temperature dependence of the MSRD's of a whole set of *different* bonds in a Debye-like system can be described with only one single parameter, ω_D, since the Debye model accounts for the displacement correlation function. For a system with a Debye phonon DOS the Einstein and Debye model fits of the MSRD of the nearest-neighbor bond are related through $\omega_E \approx 0.8\omega_D$.[54,56,63]

V. STRUCTURAL ANALYSIS

In this section we demonstrate that the local geometrical environment of the oxygen and fluorine atoms in several simple oxides and fluorides obtained from soft x-ray photoabsorption experiments is the one predicted from long-range order diffraction techniques. Based on this finding the accuracy with which nearest-neighbor bond lengths and coordination numbers can be determined from soft x-ray photoabsorption will be assessed. The improvement in distance determination established in this section with respect to earlier EXAFS analyses in the soft x-ray region has also consequences for structural determinations of low-Z adsorbates on surfaces by means of SEXAFS which will be discussed.

Figure 3 shows the $K\alpha$ fluorescence yield EXAFS spectra of CuO, Cu_2O, ZnO, CaF_2, and LiF at low temperatures. For comparison, the room-temperature data of CuO and CaF_2 are also plotted. Note that due to the stronger decay of the backscattering amplitude of the lighter elements which the fluorides consist of, the fluoride EXAFS spectra $\chi(T,k)$ are weighted with a higher power in k than the oxide ones. While little or no temperature dependence is seen in the CuO raw data, the EXAFS of CaF_2 at 300 K is strongly damped at high k values with respect to 75 K, indicating the existence of increasing MSRD's. Figure 4 shows the magnitudes of the Fourier transforms of the EXAFS spectra at low temperatures (solid lines) and at 300 K (dotted lines). It is clearly seen that the fluorides, having a larger nearest-neighbor distance than the oxides, reveal a more pronounced temperature effect whereas the first shell in the oxides is only very slightly damped. The dominant Fourier peaks of the low-temperature data in Fig. 4 (around $r = 2$ Å) were isolated by a window function and fitted in k space with theoretical standards obtained from the FEFF code[24] using an effective coordination number N^*, R, σ^2, and ΔE_0 (shift of kinetic energy zero) as fitting parameters. In the FEFF calculations, the absorbing atom was assumed to be in a fully relaxed state. The theoretical scattering amplitudes and phase shifts were found to be virtually identical for a local environment of the absorbing atom reasonably similar to the unknown one.

Care has to be taken in the k-fitting analysis of the

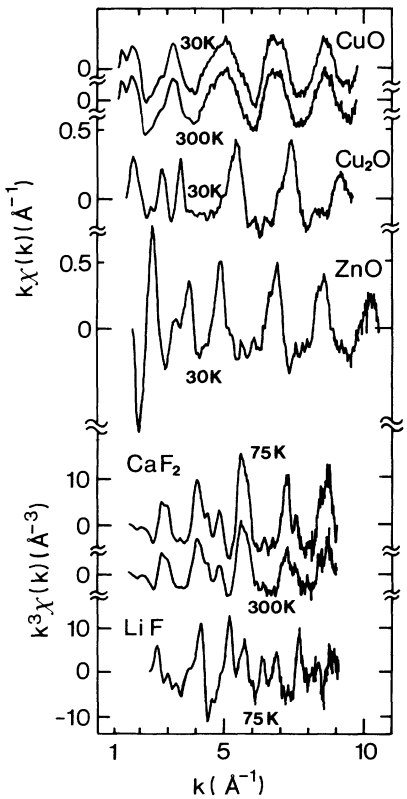

FIG. 3. Oxygen $K\alpha$ fluorescence yield EXAFS spectra of CuO, Cu_2O, and ZnO at $T = 30$ K and fluorine $K\alpha$ fluorescence yield EXAFS spectra of CaF_2 and LiF at $T = 75$ K. Note the different k weighting. For comparison, the CuO and CaF_2 EXAFS at 300 K is also plotted.

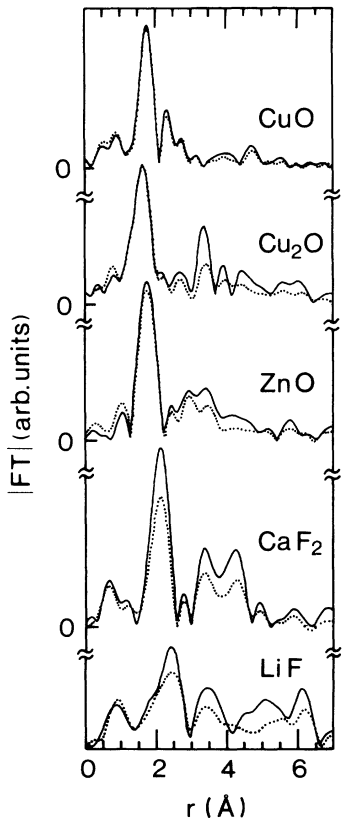

FIG. 4. Magnitudes of the Fourier transform of the EXAFS spectra of Fig. 3 at low temperatures (solid lines) and 300 K (dotted lines). A clear temperature effect is seen in the fluoride spectra, whereas the first peak of the oxide spectra almost remains unchanged.

dominant peak of the Fourier transforms in order to include all shells with considerable interference into it. In both hexagonal ZnO (Ref. 64) and cubic Cu_2O ("cuprite")[65] the closest oxygen-metal bond is more than 1.2 Å shorter than any other single- or multiple-scattering contribution to the EXAFS and, thus, a single shell fit is justified. Each central absorbing oxygen atom in both materials is tetrahedrally surrounded by four metal atoms. In Cu_2O, the O-Cu distance measured by x-ray diffraction is $R_1(30\ \text{K})=1.847(3)$ Å.[66] In the case of ZnO, the tetrahedron is slightly distorted. Nevertheless, to probe one well-defined distance, we positioned the electric field vector in single crystalline ZnO perpendicular to the c axis, eliminating the EXAFS contribution of the longer bond $R_2(30\ \text{K})=1.982(2)$ Å and examining only the three O-Zn bonds with a distance of $R_1(30\ \text{K})=1.970(2)$ Å. In this experimental geometry, the effective EXAFS coordination number remains $N^*=4$. In monoclinic CuO (Ref. 65) four Cu atoms form an angular distorted tetrahedron around each oxygen atom, but with O-Cu distances lying within 0.01 Å at $R_1(30\ \text{K})=1.954$ Å.[67] These atoms are treated here as one shell.[68] Further shells lie at $R_2(30\ \text{K})=2.623(4)$ Å (O-O, $N=2$) and $R_3(30\ \text{K})=2.774(4)$ Å (O-Cu, $N=2$), visible in the Fourier transform of Fig. 4 as the second peak around 2.4 Å. This peak seems to be well separated from the first one by the zero-intensity minimum. However, it has been pointed out that interference effects may be present even in such a situation.[69] By varying the Fourier k range and performing multiple shell fits we checked that these are weak and do not change the distance within the experimental error for CuO. Therefore, a single shell analysis appears to be appropriate. A similar argument holds for CaF_2. Only the first two shells, namely, F-Ca with $R_1(75\ \text{K})=2.358(1)$ Å ($N=4$) and F-F with $R_2(75)\ \text{K})=2.722(1)$ Å ($N=6$),[65,70] contribute to the EXAFS signal below $r=3$ Å. Figure 5(a) shows the Fourier backtransform of the first Fourier peak of CaF_2 (solid line) together with the k-fit result of a single shell of Ca atoms (circles). The agreement is very good and no evidence of a possible interference of a F-F contribution into the highly dominant F-Ca contribution is seen. Consequently, the F-Ca k-fitting results did not change significantly upon inclusion of a possible F-F contribution. This also holds for the higher moments σ^2 and c_3 of the RDF of the F-Ca bond, being most sensitive to the high-k region, since the fluorine backscattering amplitude is strongly decreasing with increasing values of k and, furthermore, the MSRD of the F-F bond is larger than that of the F-Ca bond. On the contrary, the situation appears to be more complicated for cubic LiF (sodium chloride structure).[65] To the dominant peak of the Fourier transform of Fig. 4 the weak first F-Li shell with $R_1(75\ \text{K})=2.000(1)$ Å ($N=6$) and the strong second F-F shell with $R_2(75\ \text{K})=2.827(1)$ Å ($N=12$)[65,70] do contribute, as suggested by the shoulder on the low-r side. Thus a two-shell fit has to be performed. This is illustrated in Fig. 5(b). The amplitude of the Fourier backtransform of the first Fourier peak of LiF (solid line) strongly decreases at around $k\approx 6$ Å^{-1} which cannot be accounted for by a single shell of fluorine atoms only. Instead, a two-shell fit [circles in Fig. 5(b)], the sum of a F-Li (short-dashed line) and a F-F contribution (long-dashed line), gives very good agreement with the experimental data (solid line). Because of the contributions of two different shells the ratio method is not applicable for the analysis of the dominant Fourier peak of LiF. It was not possible to obtain anharmonic information from the LiF spectra with a high degree of confidence due to the increase in the number of fitting parameters. Peaks in the Fourier transforms at higher distances, clearly seen in the spectra of Fig. 4, are found to be consistent with the known crystal structures of the compounds but are not analyzed here in detail.

Table I summarizes the structural EXAFS analysis of the first peaks of the Fourier transforms of the low-temperature spectra in Fig. 4. The nearest-neighbor distances $R_{\text{x ray}}$ and the distances R and R_{eff} obtained from the EXAFS analysis are given. As the linear term in k in the EXAFS phase, the first moment

$$R_{\text{eff}}=R(T)-\sigma^2(T)[2/R(T)+2/\lambda]$$

of the effective RDF is directly obtained as a k-fitting result. $R=R(T)$ is the true average bond length measured

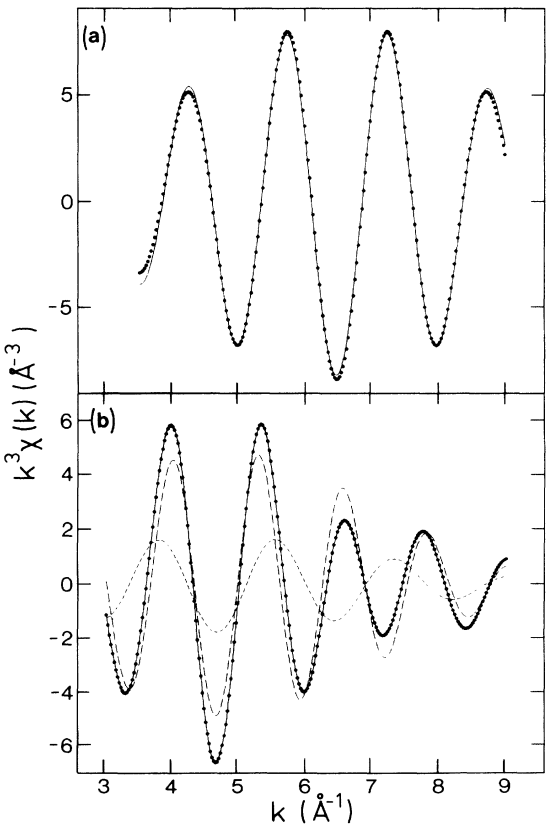

FIG. 5. Contribution of the dominant Fourier peak to the experimental CaF_2 (a) and LiF (b) EXAFS spectra at 75 K (solid lines). For CaF_2 (a), the k-fitting result of a single shell of Ca atoms gives good agreement (circles), whereas for LiF (b) a two shell fit has to performed (circles), the sum of a F-Li (short-dashed line) and a F-F contribution (long-dashed line). For the fits, theoretical standards from the FEFF code were used.

TABLE I. Nearest-neighbor distances for various oxides and fluorides as determined by EXAFS (R) and x-ray diffraction ($R_{x\ ray}$) at low temperatures. The EXAFS results are obtained from fits of the experimental data using theoretical standards from the FEFF code. R_{eff} is the uncorrected distance directly obtained from the k-fit EXAFS analysis. The amplitude reduction factor $S_0^2(\infty)$ was obtained from the EXAFS data assuming the local coordination number measured in EXAFS to take the value expected from the long-range order crystal structure. In the right column the shift of the zero kinetic energy of the photoelectron between theory and experiment is given.

Sample	T (K)	$R_{x\ ray}$ (Å)	R (Å)	R_{eff} (Å)	$N_{x\ ray}$	$S_0^2(\infty)$	ΔE_0 (eV)
CuO, 1st shell	30	1.954(5)	1.944(10)	1.941(10)	4	0.70(5)	−5.8
Cu_2O, 1st shell	30	1.847(3)	1.833(10)	1.830(10)	4	0.63(4)	−6.5
ZnO, 1st shell	30	1.970(2)	1.960(10)	1.958(10)	4	0.90(8)	−6.0
CaF_2, 1st shell	75	2.358(1)	2.372(15)	2.366(15)	4	1.00(8)	−6.1
LiF, 1st shell	75	2.000(1)	2.025(25)	2.015(25)	6	0.92(8)	−8.2
LiF, 2nd shell	75	2.827(1)	2.834(25)	2.828(25)	12	0.92(8)	3.3

by EXAFS. To yield R, the correction term

$$\sigma^2(T)[2/R(T)+2/\lambda]$$

was calculated within the Einstein model following the dynamical analysis of Sec. VI.[71] From Table I it is seen that nearest-neighbor distances obtained from x-ray diffraction and EXAFS measurements coincide within 0.015 Å. With the additional consistency of the coordination numbers (see below) we find that the local geometrical environment of the oxygen and fluorine atoms in these compounds is the one expected from long-range order diffraction techniques. The smallness of the remaining discrepancies reflects the accuracy of distance determination by means of soft x-ray photoabsorption: *High-quality fluorescence yield EXAFS data combined to theoretical standards as obtained from the* FEFF *code allow for a distance determination within 0.015 Å.*[21]

Assuming a k-independent EXAFS amplitude reduction factor $S_0^2(\infty)$ in Eq. (2a), the k-fitting analysis of the EXAFS amplitude yields $S_0^2(\infty)N^*$, N^* being the local effective coordination number of the absorbing atom measured by EXAFS.[72] In Table I, the coordination number as determined from a x-ray experiment, $N_{x\ ray}$, and the amplitude reduction factor $S_0^2(\infty)$ obtained by assuming this long-range symmetry to hold also locally, are listed. Since values of $S_0^2=0.8-0.9$ are typical,[1] Table I demonstrates that the coordination numbers measured by EXAFS agree with the crystal structure. The error bars of the EXAFS coordination numbers are limited by the actual k dependence of S_0^2 and the inclusion of absolute σ^2 values in the k-fit analysis, but not by the accuracy of the experiment. The amplitude reduction is significantly larger in the case of the Cu oxides, a fact that indicates stronger multielectron processes in these compounds. It can be concluded that at this stage of the analysis soft x-ray photoabsorption allows for a determination of coordination numbers around low-Z atoms not better than ±10–20%. In the last column of Table I, the shift ΔE_0 of the energy scale of the theoretical standard is shown which is needed to match with the experimental spectrum where the reference energy E_0 of the photoelectron kinetic energy scale is defined as the inflection point of the K edge. Values of $\Delta E_0 \approx -6$ eV are consistent with the findings for heavier atoms.[22] The negative charge at the fluorine site may cause the E_0 shift for the second shell in LiF with respect to positively charged backscatterers.

We also performed *ab initio* calculations of the *full* EXAFS of CuO, Cu_2O, ZnO, CaF_2, and LiF using clusters of the order of 100 atoms according to the x-ray diffraction structure modeling the photoelectron scattering within the first ≈10 shells around the absorbing atoms. In all cases we find very good agreement of the multiple-scattering calculations closely following the experiment (Figs. 3 and 4). These results are discussed elsewhere.[73]

The above findings have important consequences for the structural investigations of low-Z adsorbates on surfaces by means of SEXAFS. In the past, experimental standards measured by means of EY detection were used for the analysis of a number of low-Z SEXAFS data.[2,74–80] Different experimental oxygen-metal phase shifts from EY measurements were reported for Cu_2O, CuO, and NiO in the pioneering work by Stöhr,[2] which would contradict the principle of phase transferability and caused an uncertainty of about 0.05 Å in distance determinations by means of SEXAFS in the stage of 1988. In this context, a systematic deviation of distances determined by SEXAFS and LEED of this order of magnitude has been reported for some surface systems (e.g., O/Ni).[81] The experimental O-Cu phase shift determined from our present FY data is not only identical for both copper oxides (close to the one obtained in EY detection for Cu_2O) but, furthermore, agrees within 0.01 Å with the FEFF phase, see Table I.[82] As a consequence, we find the distance determinations in the systems O/Cu of Refs. 74–77 to be correct or larger than the true distance by 0.01 Å. NiO, being isostructural to LiF, was used as the experimental standard in the SEXAFS analyses of Refs. 78–80. The necessity of a two shell fit of the first Fourier peak in LiF (see above) suggests that an experimental O-Ni phase shift cannot be easily obtained from the NiO EXAFS data. However, the first Fourier peak was analyzed by conventional Fourier backtransform techniques

to give an experimental O-Ni phase shift in these studies. The O-Ni bond lengths determined from SEXAFS by this method turned out to be about 0.06 Å larger than the ones measured by other techniques.[81] A reanalysis of the SEXAFS data of the systems O/Ni (110) (Ref. 79) and $c(2\times2)$O/Ni(100) (Ref. 80) with theoretical O-Ni FEFF phase shifts removes this discrepancy completely[21]: For O/Ni(100) we get a nearest-neighbor distance of $R_{\text{O-Ni}}=1.93(2)$ Å in comparison to the low-energy electron diffraction (LEED) results that yield $R_{\text{O-Ni}}=1.92(2)$ Å (Ref. 83) and $R_{\text{O-Ni}}=1.91(2)$ Å.[81] In the case of O/Ni(110) we determine $R_{\text{O-Ni}}=1.77(3)$ Å which is exactly the value found by LEED.[84]

These examples show that the availability of accurate theoretical standards checked against high-quality fluorescence measurements clearly improves the accuracy of distance determinations by means of low-Z (S)EXAFS. The sources of error in the pioneering days of oxygen EXAFS measurements at bulk materials were (i) the limited accuracy of the EY data (normalization problems, surface nonstoichiometry due to the surface sensitivity of the method, e.g., for CuO), (ii) analysis of EXAFS spectra in terms of the single-shell single-scattering approximation despite the occurrence of shell interference and multiple-scattering effects (e.g., NiO).[21]

VI. DYNAMICAL ANALYSIS

In this section, the temperature dependence of the EXAFS spectra is investigated. Characteristic temperatures and the local thermal expansion will be determined for a variety of materials by analyzing the temperature dependence of the MSRD σ^2 and the MCRD c_3 of the nearest-neighbor shell measured by EXAFS. Except for LiF, the ratio method, see Sec. III, could be applied. Figures 6(a) and 6(b) show the logarithmic amplitude ratio

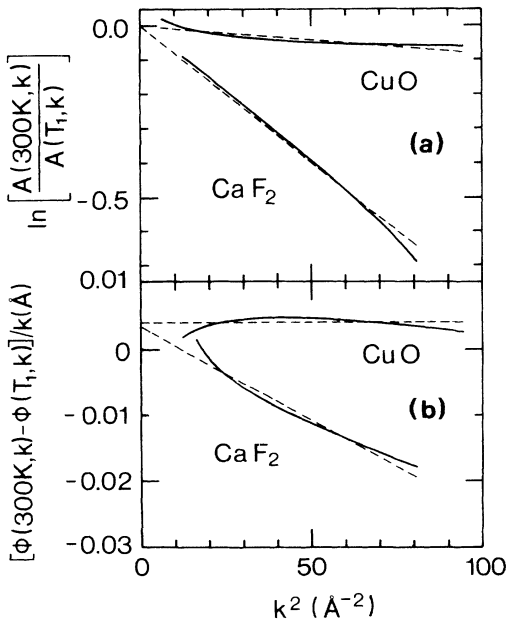

FIG. 6. Logarithmic amplitude ratio (a) and $1/k$-weighted linear phase difference (b) for CuO and CaF_2 between low temperature T_1 (30 and 75 K, respectively) and room temperature.

and $1/k$-weighted linear phase difference plots for CuO and CaF_2 between low temperature T_1 (30 K and 75 K, respectively) and room temperature. The CaF_2 data exhibit a much stronger temperature dependence than the CuO ones, as was already seen qualitatively in Figs. 1–4. According to Eq. (3), from the slopes of the straight lines in Figs. 6(a) and 6(b) the relative changes of σ^2 and c_3 are determined to be

$$\Delta\sigma^2(300\text{ K},\ 30\text{ K})=0.4(3)\times10^{-3}\text{ Å}^2$$

and

$$\Delta c_3(300\text{ K},\ 30\text{ K})=0.0(4)\times10^{-4}\text{ Å}^3$$

in CuO and

$$\Delta\sigma^2(300\text{ K},\ 75\text{ K})=3.9(3)\times10^{-3}\text{ Å}^2$$

and

$$\Delta c_3(300\text{ K},\ 75\text{ K})=2.1(4)\times10^{-4}\text{ Å}^3$$

in CaF_2. As discussed in Sec. IV, each of these pairs of dynamic quantities allows us to determine the harmonic force constant γ and the cubic anharmonicity constant β of the effective pair potential assumed to describe the pair interaction of the absorbing and backscattering atom [Eq. (7)]. Instead of γ, the Einstein temperature Θ_E, being proportional to the square root of γ, can be used as a parameter [Eq. (10)]. Together with the low-temperature nearest-neighbor distance $R(T_1)$ the full temperature dependence of all dynamic quantities, including the thermal expansion, can be obtained [Eqs. (6)–(11)].

Tables II and III give a full compilation of the results of the first shell dynamic EXAFS analysis of our fluorides and oxides and, in comparison, of various surface systems, fcc metals, superionic conductors, and alkali halides, analyzed in exactly the same manner. These tables include all temperature-dependent EXAFS studies in the literature we were aware of where anharmonicity is quantitatively reported in terms of Δc_3. It is emphasized that all parameters in the Tables II and III are derived only from EXAFS data at *two distinct* temperatures, a low temperature $T_1\leq100$ K and $T_2\approx300$ K. Table II lists the bond measured by EXAFS, the reduced mass μ of the atom pair forming this bond, the experimentally measured changes in the dynamic parameters $\Delta\sigma^2(T_2,T_1)$ and $\Delta c_3(T_2,T_1)$ between the temperatures T_2 and T_1, and the potential parameters r_0, γ, and β obtained from a fit of $\Delta\sigma^2(T_2,T_1)$, $\Delta c_3(T_2,T_1)$ and $R(T_1)$ to the anharmonic oscillator model using Eqs. (6)–(10). Table III contains the characteristic Einstein and Debye temperatures, Θ_E and Θ_D^{ex}, determined by EXAFS, compared to the calorimetrically measured values $\Theta_D^c(0\text{ K})$, $\Theta_D^c(T_1)$, and $\Theta_D^c(T_2)$, the ratio $\Theta_E/\Theta_D^c(0\text{ K})$ and the coefficient of the linear local thermal expansion $\alpha_{\text{ex}}(T_2)$ determined by EXAFS at the temperature T_2 (see Table II) in comparison to the value $\alpha(T_2)$ measured by other techniques, like x-ray diffraction. To our knowledge this is the most extended compilation to date of the dynamical parameters obtained by means of EXAFS. Such a systematic comparison for a variety of different materials

is necessary in order to estimate the accuracy of local thermal expansion measurements by use of EXAFS.

We now discuss the entries of the Tables II and III for CaF_2 and CuO, two representative examples. The other compounds are analyzed similarly. We first focus on the discussion of the characteristic temperatures. The Einstein temperature Θ_E (and also the harmonic force constant γ) is entirely determined through the value of $\Delta\sigma^2(T_2,T_1)$. For CaF_2, we obtain $\Theta_E=377(10)$ K. Assuming the anharmonicity to be a weak perturbation only, we performed also Debye fits to the measured $\Delta\sigma^2(T_2,T_1)$ according to Ref. 53. The Debye model was derived from monoatomic, cubic species and therefore the transfer to biatomic compounds may introduce errors. In all our Debye fits of biatomic crystals we set the atomic mass to the mean value of the atoms *within a unit cell of the crystal,* as was also done in Ref. 60. For CaF_2, for example, one gets $M=26.03$ amu and the harmonic Debye fit of $\Delta\sigma^2$ yields $\Theta_D^{ex}=490(20)$ K, compared to a calorimetrically measured $\Theta_D^c(0\text{ K})=506(6)$ K.[85–87] The Debye approximation can therefore be used to describe the CaF_2 phonon DOS in the EXAFS experiment, although the true phonon DOS considerably differs from the Debye behavior at higher phonon frequencies.[87] A ratio of $\Theta_E/\Theta_D^c(0\text{ K})=0.75(3)$ is obtained, close to the value of a Debye system.[54,56] This ratio can be considered as a measure of the "Debye character" of the phonon DOS as probed by EXAFS. The change in the MSRD of the first shell in CuO is an order of magnitude smaller than in CaF_2 yielding a higher Einstein temperature of $\Theta_E\geq 660$ K. The change in the MSRD's in all the oxides under investigation is below 5×10^{-4} Å^2 between low and room temperature, of the same order as the experimental error. Therefore, only lower limits of the characteristic temperatures in our oxides could be deter-

TABLE II. Differences in the mean-square and mean-cubic relative displacements, $\Delta\sigma^2$ and Δc_3, between the temperatures T_1 and T_2 as measured by EXAFS. The measured bond (first atom is the absorber) and the reduced mass μ of the atom pair forming this bond are listed. The three columns on the right show the parameters of the effective pair potential of the bond [Eq. (7)], namely, r_0 (potential minimum), γ (harmonic force constant), and β (anharmonic constant), obtained from an anharmonic Einstein model fit to the values $\Delta\sigma^2$, Δc_3 and the low-temperature EXAFS distance $R(T_1)$. The physical constants of Table III are calculated with these Einstein model parameters. They are very insensitive to the absolute values of r_0. The entry "mean" in the "bond" column denotes the average of the EXAFS results obtained from the absorption edges of the two different atomic species forming the nearest-neighbor bond, as in a binary compound the physical parameters of Table III do not depend on the specific site. O/Cu^+ and O/Cu^* are the two different adsorption states of oxygen on Cu(100) (Ref. 100). The entries in square brackets are calculated from the coefficient of thermal expansion $\alpha(300\text{ K})$ measured by other techniques (see Table III). The few lattice-dynamical calculations of $\Delta\sigma^2$ existing in the literature are in fair agreement with the experimental values of this table: $\Delta\sigma_t^2(295\text{ K},80\text{ K})=4.4\times10^{-3}$ Å^2 for Cu (Ref. 54), $\Delta\sigma_t^2(300\text{ K},110\text{ K})=2.9\times10^{-3}$ Å^2 for Pt (Ref. 54), and $\Delta\sigma_t^2(300\text{ K},100\text{ K})=1.63\times10^{-3}$ Å^2 for O/Ni (Ref. 109).

Sample	Reference	Bond	μ (amu)	T_1 (K)	T_2 (K)	$\Delta\sigma^2(T_2,T_1)$ (10^{-3} Å^2)	$\Delta c_3(T_2,T_1)$ (10^{-4} Å^3)	r_0 (Å)	γ (eV Å^{-2})	β (eV Å^{-3})
CaF_2	This	F-Ca	12.89	75	300	3.9(3)	2.1(4)	2.365	3.3(2)	2.1(7)
LiF	This	F-Li	5.08	75	300	3.3(4)	[3.9]	2.027	2.7(2)	[2.6]
LiF	This	F-F	9.50	75	300	4.6(4)	[5.5]	2.836	2.7(2)	[3.0]
ZnO	This	O-Zn	12.85	30	300	0.1(4)	0[≤0.1]	1.960	≥12	[≥7]
CuO	This	O-Cu	12.78	30	300	0.4(3)	0[≤0.3]	1.945	≥10	[≥11]
Cu_2O	This	O-Cu	12.78	30	300	0.3(3)	0[≤0.05]	1.834	≥11	[≥2.5]
O/Cu^+	25,26	O-Cu	12.78	50	300	4.6(5)	2.6(2)	1.858	2.9(2)	1.8(6)
O/Cu^*	100	$O\text{-}Cu_{\parallel}$	12.78	50	300	0.9(3)	0.5(2)	1.833	9(2)	
O/Cu^*	100	$O\text{-}Cu_{\perp}$	12.78	50	300	10.2(3)	7.6(3)	2.049	1.6(1)	0.8(1)
O/Ni	26	O-Ni	12.57	50	300	2.5(3)	1.7(3)	1.913	4.5(4)	5(2)
N/Ni	100,26	$N\text{-}Ni_{\parallel}$	11.31	50	300	1.3(4)	0.7(3)	1.874	7(1)	7(5)
N/Ni	100,26	$N\text{-}Ni_{\perp}$	11.31	50	300	0.8(4)	0.3(3)	1.846	9(3)	
N/Cu	102	N-Cu	11.48	30	300	3.5(4)	1.8(3)	1.848	3.5(3)	2.2(9)
Cu	27	Cu-Cu	31.77	80	295	5.1(2)	1.3(2)	2.548	3.1(1)	1.0(3)
Ag	27	Ag-Ag	53.93	30	360	9.1(2)	4.6(2)	2.875	2.67(5)	1.6(2)
Au	27	Au-Au	98.48	80	295	6.3(2)	1.9(2)	2.876	2.8(1)	1.1(2)
Pt	This	Pt-Pt	97.50	110	300	3.2(2)	0.6(2)	2.774	4.8(2)	2(1)
Pd	27,37	Pd-Pd	53.2	100	295	3.7(2)	0.9(2)	2.745	4.0(2)	1.8(6)
Pb	40	Pb-Pb	103.6	10	300	24(3)	12(3)	3.490	1.0(1)	0.3(1)
NaBr	35	Br-Na	17.85	71	295	18(2)	17(2)	2.975	0.97(8)	0.4(1)
RbBr	30	Rb-Rb	42.74	30	125	9(1)	5.9(3)	4.806	0.73(7)	0.4(1)
RbCl	35	Rb-Cl	25.06	71	295	18(1)	9(2)	3.283	1.00(7)	0.25(9)
CuBr	34	Mean	35.40	72	295	8.0(7)	3.7(5)	2.456	2.1(2)	1.0(4)
	27	Mean	35.40	50	295	8.8(9)	5(1)	2.456	2.0(2)	1.1(6)
	38	Br-Cu	35.40	20	300	6(1)	4(1)	2.456	3.1(4)	3(2)
AgBr	27	Mean	45.90	50	295	17(1)	12(2)	2.865	1.16(6)	0.5(1)
AgI	39	Ag-I	58.21	73	373	15(2)	3(1)	2.813	1.6(2)	0.2(1)

mined. In order to determine the characteristic temperatures accurately, measurements at temperatures of several hundred degrees Celsius would have to be performed. The temperature dependence of the MSRD of the O-Cu bond has also been measured by means of Cu K edge EXAFS.[88,89] In these studies, an Einstein temperature of $\Theta_E = 680(50)$ K and $\Theta_E = 620(20)$ K was determined, respectively, consistent with the lower limit we estimated from our measurements. Our CuO data also yield a lower limit of the Debye temperature of $\Theta_D^{ex} \geq 750$ K, considerably different from the calorimetric value of $\Theta_D^c = 400-570(20)$ K.[90-93] The origin of this discrepancy is discussed in Sec. VII in context to the CuO phonon DOS and also the other compounds of Table III. It should be noted already that CuO is paramagnetic at 300 K. At 230 and 212 K CuO undergoes two antiferromagnetic phase transitions into an incommensurate and commensurate spin state, respectively.[90-94] However, only little coupling between magnetic and structural behavior was found; peaks occurring in the specific heat[90-93] and in the coefficient of the bulk thermal expansion[95] have only $\approx 5\%$ relative intensity. Therefore, although measuring the EXAFS in CuO in two different phases, the ratio method can be applied to gain temperature dependent structural information far away from the phase transition.

The parameter β of the anharmonic contribution to the effective pair potential as well as the thermal expansion can be obtained from the value of $\Delta c_3(T_2, T_1)$ since Θ_E is known [Eqs. (8) and (11)]. A coefficient of the linear thermal expansion at room temperature of $\alpha_{ex}(300\ \text{K}) = 1.9(5) \times 10^{-5}\ \text{K}^{-1}$ is obtained for CaF_2, in very good agreement with other techniques like x-ray diffraction yielding $1.9(2) \times 10^{-5}\ K^{-1}$.[70] For CuO, and also the other oxides under investigation, the change in Δc_3 between low temperature and 300 K is below 4×10^{-5} Å^3 and, within the experimental accuracy, not detectable. Other techniques show that the thermal expansion in the oxides is smaller not only at 300 K but in the high-temperature limit as well than in all the other systems under investigation (see Table III).[66,70,95] The entries in square brackets given in Table II for $\Delta c_3(T_2, T_1)$ have been calculated from these thermal expansion values and are indeed found to be smaller than the experimental sensitivity.

As discussed in Sec. IV, in principle, it is possible to

TABLE III. Characteristic Debye (Θ_D) and Einstein (Θ_E) temperatures and coefficients of the linear thermal expansion (α) measured by EXAFS in comparison with other techniques. The superscript c denotes values from calorimetric measurements and the superscript ex denotes EXAFS measurements. The last column gives the high-temperature saturation value of the coefficient of the linear thermal expansion obtained from EXAFS. References for the calorimetric Debye temperatures, the thermal expansion and the phonon DOS for the materials in the table are (in this order) as follows: Refs. 85–87, 70, 87 (CaF_2); 103–105, 70, 103–105 (LiF); –,70,– (ZnO); 90–93, 95, 91 (CuO); –, 66, – (Cu_2O); 96, 70, 96 (Cu, Ag, Au); 106, 70, 96 (Pt, Pd); 106, 40, 96 (Pb); 103, 70, – (NaBr, RbBr, RbCl); 107, 70, 107 (CuBr); and –, 70, – (AgBr, AgI).

Sample	Bond	Θ_E (K)	Θ_D^{ex} (K)	Θ_D^c (0 K) (K)	$\Theta_D^c(T_1)$ (K)	$\Theta_D^c(T_2)$ (K)	$\Theta_E / \Theta_D^c(0\ \text{K})$	$\alpha_{ex}(T_2)$ ($10^{-5}\ \text{K}^{-1}$)	$\alpha(T_2)$ ($10^{-5}\ \text{K}^{-1}$)	α_{ex}^{cl} ($10^{-5}\ \text{K}^{-1}$)
CaF_2	F-Ca	377(10)	490(20)	506(6)	480(4)	504(10)	0.75(3)	1.9(5)	1.9(2)	2.1(5)
LiF	F-Li	550(20)	675(30)	730(40)	610(20)	630(20)	0.75(8)		3.4(3)	
LiF	F-F	397(10)	679(20)	730(40)	610(20)	630(20)	0.54(5)		3.4(3)	
ZnO	O-Zn	≥730	≥800						0.45(5)	
CuO	O-Cu	≥660	≥750	395(20)	400(20)	575(20)	≥1.1		0.75(9)	
Cu_2O	O-Cu	≥690	≥690						0.2(1)	
O/Cu^+	O-Cu	360(20)						2.6(4)		2.9(5)
O/Cu*	$O\text{-Cu}_{\parallel}$	620(60)						1.4(9)		2(1)
O/Cu*	$O\text{-Cu}_{\perp}$	263(5)						3.8(3)		4.0(3)
O/Ni	O-Ni	450(20)						2.6(6)		3.1(7)
N/Ni	$N\text{-Ni}_{\parallel}$	570(50)						1.7(9)		2(1)
N/Ni	$N\text{-Ni}_{\perp}$	660(90)						1(1)		2(2)
N/Cu	N-Cu	410(20)						2.2(5)		2.5(6)
Cu	Cu-Cu	232(5)	317(5)	346(2)	317(2)	320(5)	0.67(2)	1.1(2)	1.6(1)	1.1(2)
Ag	Ag-Ag	167(2)	228(2)	227(2)	210(2)	220(10)	0.74(2)	1.9(1)	1.85(5)	2.0(1)
Au	Au-Au	126(2)	172(3)	162(5)	183(2)	190(20)	0.78(3)	1.3(2)	1.40(5)	1.3(2)
Pt	Pt-Pt	166(5)	226(7)	240			0.69	0.8(3)	0.90(5)	0.8(3)
Pd	Pd-Pd	207(5)	282(7)	274(4)			0.76(3)	1.0(3)	1.2(1)	1.0(3)
Pb	Pb-Pb	72(4)	98(6)	105			0.69	2.1(8)	3.0(2)	2.1(8)
NaBr	Br-Na	175(8)	190(8)	225(1)			0.78(4)	3.9(8)	4.0(3)	4.0(8)
RbBr	Rb-Rb	98(5)	147(7)	136(3)			0.72(5)	3.4(5)	3.7(3)	3.6(5)
RbCl	Rb-Cl	150(5)	176(6)	167(2)		157	0.90(4)	1.9(5)	3.6(3)	2.0(5)
CuBr	Mean	184(7)	214(9)	160(10)	200(10)	210(20)	1.2(1)	2.2(5)	1.4(2)	2.3(5)
	Mean	180(8)	211(10)	160(10)	195(10)	210(20)	1.1(1)	2.6(9)	1.4(2)	2.7(9)
	Br-Cu	220(20)	265(20)	160(10)	136(10)	210(20)	1.4(2)	3(1)	1.4(2)	3(1)
AgBr	Mean	119(3)	151(4)					3.3(6)	3.4(3)	3.4(6)
AgI	Ag-I	[126(8)]	[150(10)]					[0.8(3)]		[0.8(3)]

determine the net local thermal expansion through the linear term in the EXAFS phase or, equivalent, by the intercept of the $1/k$-weighted phase difference plot of Fig. 6(b). Using this method we obtain with the values of Table II for CaF_2 $\Delta R(300\text{ K}, 75\text{ K}) = 0.006(4)$ Å,[71] in comparison to 0.0075(7) Å measured by x-ray diffraction.[70] The calculation of $\Delta R(300\text{ K}, 75\text{ K})$ by use of the anharmonic Einstein model of Table II gives the more precise value of 0.008(2) Å. For CuO, the net thermal expansion is determined from the linear term in the EXAFS phase as $\Delta R(300\text{ K}, 30\text{ K}) = 0.003(4)$ Å in comparison to 0.0022 Å measured with a capacitance dilatometer.[95] Our results for CaF_2 confirm that the relative error of $\geq 50\%$ of the local thermal expansion determined through the linear term of the EXAFS phase is considerably larger than the error obtained by evaluating $\Delta\sigma^2$ and Δc_3 within the anharmonic Einstein model.

VII. COMPARATIVE DISCUSSION OF THE DYNAMICAL QUANTITIES

We start the discussion with the fcc metals, rows "Cu" to "Pb" in Table III. It is observed that the Debye temperatures of the nearest-neighbor bonds determined from EXAFS agree with the calorimetric measurements. This finding is not surprising as the Debye model approximates the true phonon DOS of fcc metals quite well[96] and the Debye temperature of an ideal Debye system would coincide with the one measured in EXAFS and calorimetry. For the same reason, the ratio of the Einstein temperature Θ_E and the 0 K calorimetric Debye temperature $\Theta_D^c(0\text{ K})$ approaches the value 0.8 quite well.[54,56] However, as an EXAFS measurement is sensitive only to relative atomic motions (i.e., the projected density of states[1]), EXAFS and calorimetric Debye temperatures are different, in general. This is the case when the correlated atomic motion cannot be adequately described using the Debye approximation.[53] Below this is illustrated by the binary compounds like CuO, where the difference can be linked to the deviation of the phonon DOS from the Debye model. The discrepancy between EXAFS and calorimetric Debye temperatures in the case of copper is not discussed in Ref. 27. The Einstein temperatures of the nearest-neighbor bonds in the fcc metals determined in Table III from the EXAFS measurements at two temperatures are found to agree with the more extended Einstein fits of Ref. 56.

$\alpha_{ex}(T_2)$ and $\alpha(T_2)$ of Table III show that the coefficients of the thermal expansion obtained from EXAFS and other techniques agree within the error for fcc metals (except for the copper data). In sufficiently complex systems, the local thermal expansion of a particular bond measured by EXAFS is, of course, different from the average macroscopic thermal expansion determined by x-ray diffraction and other techniques. A spectacular example is the local premelting around mercury impurities in bulk lead reported recently.[36] For the simple cubic metals and binary compounds of Table III, however, the macroscopic thermal expansion is independent of the crystal orientation. Since in all cases chains of the particular bond measured by EXAFS progress through the whole crystal, *the local thermal expansion probed by EXAFS can be assumed to be identical to the macroscopically measured one for the compounds listed in Table III.* It is again pointed out that the effect of correlated motion of the absorbing and backscattering atom in the EXAFS experiment (i.e., the displacement correlation function) is not taken into account in the *derivation* of the Einstein model but is implemented later through the fit of the Einstein temperature Θ_E to the measured MSRD. The anharmonic Einstein model with its parameters Θ_E or γ, β, and r_0 reproduces the experimentally measured functional behavior of $\sigma^2(T)$ and $c_3(T)$ correctly *in the case of weak anharmonicity* and therefore yields within the accuracy of the model also the *true local thermal expansion,* i.e., the elongation $R(T)-R(0\text{ K})$ of the bond length, and the coefficient $\alpha(T)$ of the linear local thermal expansion. As obtained from the anharmonic Einstein model, the latter one follows a specific-heat-like curve, saturating to the classical value α^{cl} at high temperatures $T \gg \Theta_E$. From Eq. (11) one obtains

$$\alpha^{cl} = \frac{3\hbar^4\beta}{R(0\text{ K})\mu^2 k_B^3 \Theta_E^4} = \frac{3k_B\beta}{R(0\text{ K})\gamma^2} . \tag{12}$$

Θ_E being of the order of room temperature, the thermal expansion measured at 300 K for the systems of Table III is lower than the high-temperature limit to a different degree for each of the systems, since $T = 300$ K corresponds to different reduced temperatures T/Θ_E. Therefore, a fair comparison of absolute values of thermal expansion or anharmonicity is given by its high-temperature limit which is shown in the right-most column of Table III. The fcc metals and the binary compounds given below behave to within 5% classically at 300 K whereas for the samples with higher characteristic temperatures like surface systems and oxides the difference is about 30%.

The discrepancy between EXAFS and calorimetric Debye temperatures for the binary compounds is considerably larger than for the metals which is caused by a stronger deviation of their phonon DOS from the Debye behavior. This is also reflected by the larger temperature variation of the calorimetric Debye temperature. As an extreme example, the difference between EXAFS and calorimetric Debye temperature for CuO can be related to its phonon DOS by the following simple picture. The CuO phonon DOS is highly dominated by a series of sharp peaks,[91] leaving only a very small but steep parabolic onset at low phonon frequencies. This steep parabolic onset results in a 0 K Debye frequency for CuO of $\omega_D(0\text{ K}) = 51.6$ THz, far below the cutoff frequency of the phonon spectrum of 122 THz. For silver, in comparison, the value of $\omega_D(0\text{ K}) = 29.7$ THz almost agrees with the phonon cutoff frequency of ≈ 32 THz.[96] Also in other binary compounds like LiF and CaF_2, the parabolic onset is broader and Debye and cutoff frequencies differ only by $\approx 30\%$. The EXAFS measurement is monitoring the relative atomic motions and therefore is most sensitive to high frequency optical-type phonons. Consequently, the MSRD of EXAFS freezes out for CuO at higher temper-

atures than the Debye temperature and a higher EXAFS Debye temperature is obtained.

The coefficients of the local linear thermal expansion measured by EXAFS and other techniques agree well for the binary compounds CaF_2, NaBr, RbBr, and AgBr, the later ones being known as quite strong anharmonic systems. On the contrary, the values for RbCl and CuBr clearly differ. The reason for this discrepancy is not clear presently; it neither seems to be correlated to the atomic mass difference in the compounds nor to the absolute magnitude of the thermal expansion. Further investigations are needed to clarify this point. AgI exhibits a negative thermal expansion below room temperature[70] and the assumption of a weak perturbation of the harmonic potential appears to be problematic. The parameters obtained from the anharmonic Einstein model are therefore given in brackets in Table III.

Taking advantage of the very local and specific view of EXAFS, the dynamics, anharmonicity, and local thermal expansion of adsorbates on surfaces can be determined from surface EXAFS measurements. Evidence for anharmonic interactions on surfaces has been found for several surface systems[97–99] and in Ref. 26 the local thermal expansion of various surface and bulk systems has been classically calculated starting from Eq. (5). In Table III, the quantum-mechanical reanalysis of these and additional surface systems based on the anharmonic Einstein model is included. O/Cu^+ and O/Cu* denote the two different atomic chemisorption states found for oxygen on Cu(100),[100] the precursor state and the missing-row reconstructed state, respectively. Through angular dependent surface EXAFS experiments bonds lying within the substrate surface plane and perpendicular can be separately sampled, as denoted by the subscripts in Table III. It is seen that these adsorbates on surfaces are characterized by (i) high Einstein temperatures typically lying far above room temperature and (ii) large coefficients of thermal expansion, comparable to the ones of quite strong anharmonic bulk systems like alkali and metal halides. The corresponding bulk oxides Cu_2O, CuO, and NiO (the latter one not presented here) show significantly smaller thermal expansion,[66,95] among the weakest known for bulk materials and not detectable in our EXAFS measurements up to 300 K. This clearly confirms the recent finding of enhanced anharmonicity in the adsorbate-surface interaction which was suggested to be an intrinsically surface-related phenomenon.[26]

Figure 7 shows a double logarithmic correlation diagram of the parameters γ and β of the effective pair interaction potential between the absorbing and backscattering atom obtained by an anharmonic Einstein model fit to the EXAFS data (see Table II and Sec. IV). From Eq. (12) it is seen that all compounds with the same high-temperature saturation value of the coefficient of local linear thermal expansion lie on a straight line with a slope of 2 in this diagram. This saturation value is obtained as the $\gamma = 1$ eV Å^{-2} intercept of the lines (see dashed line in Fig. 7) and is also listed in the right-most column of Table III. The error bars of the potential parameter β in Fig. 7 are relatively large and have not been included. They can be obtained from Table II. We

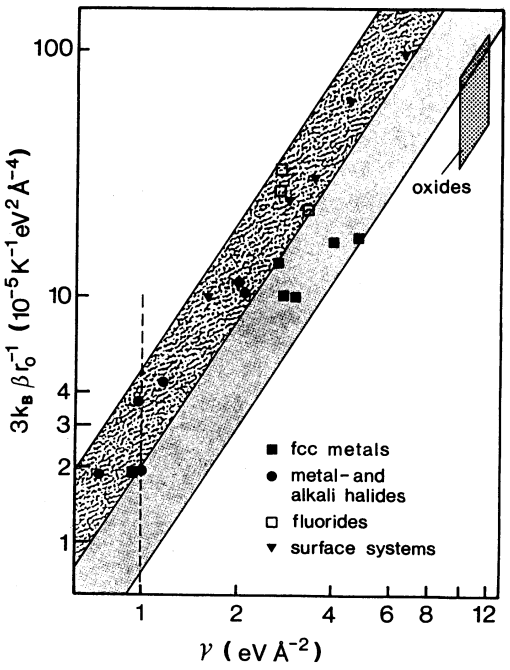

FIG. 7. Double logarithmic correlation diagram of γ versus $3k_B\beta/r_0$. γ and β are the harmonic force constant and the anharmonicity constant of the anharmonic pair interaction potential [Eq. (7)] between absorbing and backscattering atom. The upper (textured) and lower (grey) regions mark different high-temperature saturation values of the coefficient of linear thermal expansion of above and below 2×10^{-5} K^{-1} which can be read from the $\gamma = 1$ eV Å^{-2} intercept (dashed line). Within the dotted area bulk oxides are located. See text for further discussion.

marked two different regions in Fig. 7, corresponding to high-temperature saturation values of the coefficient of the linear local thermal expansion above (upper, textured area) and below 2×10^{-5} K^{-1} (lower, grey area). In the lower area at γ values of around 3–4 eV Å^{-2} typical fcc metals are located. The upper area contains the stronger anharmonic compounds such as metal and alkali halides, the light fluorine compounds and the surface systems. It should be noted that the adsorbate-substrate bonds of the surface systems have typically much larger harmonic force constants γ, i.e., are stronger, than the fluoride and especially the metal- and alkali-halide ones. Because of the low mass of the adsorbates this is through Eq. (10) correlated to much higher Einstein temperatures of the surface systems. The bulk oxides (dotted region on the right-hand side of Fig. 7) have even stronger harmonic force constants, but anharmonicity constants β comparable to the surface systems. This illustrates again the different pair interaction in the bulk and at surfaces.

VIII. CONCLUSION

We have presented the structural and dynamical analysis of temperature-dependent *fluorescence* EXAFS measurements at the oxygen and fluorine *K* edges of various oxides and fluorides. A state-of-the-art EXAFS

analysis of bulk compounds in the soft x-ray region of $h\nu \leq 1.5$ keV, meeting the quality of EXAFS analyses in the harder x-ray region, demonstrates in detail that the *character* of the information obtainable is identical in both regions, but usually with a somewhat larger error in the soft x-ray regime. This is due to the typically smaller k range of the soft x-ray data. In particular, we showed that soft x-ray photoabsorption yields accurate structural information around light elements in bulk compounds and for adsorbates on surfaces, e.g., bond distances within 0.015 Å. A by-product of the present investigation is the confirmation of the transferability of the EXAFS phase shift in copper oxides. In S-Ni systems, this question was also addressed recently.[101] The temperature dependence of the spectra provides detailed dynamical information such as atomic mean-square relative displacements and asymmetry of the radial pair distribution function of the bond under consideration. Anharmonicity effects in soft x-ray EXAFS of bulk compounds were quantitatively reported and analyzed. Within the framework of quantum-mechanical models characteristic temperatures and the local thermal expansion of the bonds were obtained. A detailed systematic comparative analysis with respect to these quantities was given for CaF_2, LiF, transition-metal oxides, and, furthermore, the majority of materials for which anharmonicity effects have been quantitatively examined in the EXAFS literature. We argued that local and macroscopic thermal expansion are expected to be identical for the simple cubic compounds investigated here which is confirmed for fcc metals. Agreement is also obtained for the binary compounds CaF_2, NaBr, RbBr, and AgBr, whereas for RbCl and CuBr a discrepancy is observed the origin of which is not yet understood. Therefore, further experiments are desirable in order to explore in more detail also the accuracy of the determination of the thermal expansion by means of EXAFS, in our analysis of the order of 20%.

This study helps to establish soft x-ray photoabsorption as a tool for the investigation of structural and dynamical properties of light elements in bulk materials in two ways: (i) for well-known model systems, as studied here, the local properties on an atomic scale can be studied more clearly, (ii) once the method is established materials with unknown local structure and interaction, as ceramics, can be investigated. We mention that in certain cases limitations of this technique do exist. In the energy range of $h\nu \leq 1500$ eV many L-, M-, and N-absorption edges of heavier atoms are located. Depending on the stoichiometry of the sample this can limit the energy range over which the x-ray absorption fine structure of the light element of interest can be recorded. The favorable fluorescence detection method may be able to overcome these limitations, since in some cases it can be employed to extend the measurement of the EXAFS even *above* higher energy absorption edges by means of a compensation technique.[108]

ACKNOWLEDGMENTS

We acknowledge fruitful discussions with J. J. Rehr, H. Rabus, and C. Dagg. We thank J. J. Rehr also for making Ref. 30 available to us prior to publication. We thank the BESSY staff for the help during the experiments. We are especially grateful to S. Hüfner for supplying the CuO and Cu_2O samples. The work was supported by the German BMFT under Grant No. 05 5KEAAB and F&E-Vorhaben 13N5740.

[1]See, for instance, *X-Ray Absorption: Principles, Applications, Techniques of EXAFS, SEXAFS and XANES,* edited by R. Prins and D. C. Koningsberger (Wiley, New York, 1988).

[2]See J. Stöhr, in *X-Ray Absorption: Principles, Applications, Techniques of EXAFS, SEXAFS and XANES,* edited by R. Prins and D. C. Koningsberger (Wiley, New York, 1988), and the references therein.

[3]A. P. Lukirskii and I. A. Brytov, Sov. Phys. Solid State **6**, 33 (1964).

[4]W. Gudat and C. Kunz, Phys. Rev. Lett. **29**, 169 (1972).

[5]W. Gudat, Ph.D. thesis, Universität Hamburg, Germany, 1974.

[6]G. Martens, P. Rabe, N. Schwentner, and A. Werner, J. Phys. C **11**, 3125 (1978).

[7]P. H. Citrin, P. Eisenberger, and R. C. Hewitt, Phys. Rev. Lett. **41**, 309 (1978).

[8]D. Denley, R. S. Williams, P. Perfetti, D. A. Shirley, and J. Stöhr, Phys. Rev. B **19**, 1762 (1979).

[9]J. Jaklevic, J. A. Kirby, M. P. Klein, A. S. Robertson, G. S. Brown, and P. Eisenberger, Solid State Commun. **23**, 679 (1977).

[10]D. A. Fischer, U. Döbler, D. Arvanitis, L. Wenzel, K. Baberschke, and J. Stöhr, Surf. Sci. **177**, 114 (1986); D. Arvanitis, U. Döbler, L. Wenzel, K. Baberschke, and J. Stöhr, J. Phys. (Paris) Colloq. **47**, C8-173 (1986).

[11]F. Riehle, E. Tegeler, and B. Wende, Soft X-Ray Opt. Technol. **733**, 486 (1986).

[12]M. Krumrey, E. Tegeler, and G. Ulm, Rev. Sci. Instrum. **60**, 2287 (1989).

[13]G. C. Smith, A. Krol, and Y. H. Kao, Nucl. Instrum. Methods Phys. Rev. A **291**, 135 (1990).

[14]L. Tröger, D. Arvanitis, H. Rabus, L. Wenzel, and K. Baberschke, Phys. Rev. B **41**, 7297 (1990).

[15]L. Tröger, D. Arvanitis, K. Baberschke, H. Michaelis, U. Grimm, and E. Zschech, Phys. Rev. B **46**, 3283 (1992); L. Tröger, E. Zschech, D. Arvanitis, and K. Baberschke, Jpn. J. Appl. Phys. **32**, Suppl. **32-2**, 144 (1993).

[16]Y. H. Kao, L. Y. Jang, W. Ng, A. Krol, S. C. Woronick, F. Xu, and Y. D. Yao, Physica B **158**, 488 (1989).

[17]A. Krol, C. S. Lin, Z. H. Ming, C. J. Sher, Y. H. Kao, C. T. Chen, F. Sette, Y. Ma, G. C. Smith, Y. Z. Zhu, and D. T. Shaw, Phys. Rev. B **42**, 2635 (1990).

[18]L. Tröger, D. Arvanitis, H. Rabus, K.Baberschke, and B. Stritzker, in *X-Ray Absorption Fine Structure,* edited by S. Samar Hasnain (Ellis Horwood, Chichester, England, 1991), p. 616.

[19]D. A. Fischer, G. Meitzner, and J. Gland, in *X-Ray Absorption Fine Structure,* edited by S. Samar Hasnain (Ellis Horwood, Chichester, England, 1991), p. 619.

[20]E. Zschech, L. Tröger, D. Arvanitis, H. Michaelis, U. Grimm, and K. Baberschke, Solid State Commun. **82**, 1 (1992).
[21]L. Tröger, D. Arvanitis, J. J. Rehr, T. Lederer, T. Yokoyama, K. Baberschke, and E. Zschech, Jpn. J. Appl. Phys. **32**, Suppl. **32-2**, 137 (1993).
[22]J. J. Rehr, J. Mustre de Leon, S. I. Zabinsky, and R. C. Albers, J. Am. Chem. Soc. **113**, 5135 (1991); J. Mustre de Leon, J. J. Rehr, S. I. Zabinsky, and R. C. Albers, Phys. Rev. B **44**, 4146 (1991).
[23]J. J. Rehr and R. C. Albers, Phys. Rev. B **41**, 8139 (1990).
[24]J. J. Rehr, R. C. Albers, and S. I. Zabinsky, Phys. Rev. Lett. **69**, 3937 (1992).
[25]L. Wenzel, Ph.D. thesis, Freie Universität Berlin, Germany, 1989, p. 67.
[26]L. Wenzel, D. Arvanitis, H. Rabus, T. Lederer, and K. Baberschke, Phys. Rev. Lett. **64**, 1765 (1990); H. Rabus, D. Arvanitis, T. Lederer, and K. Baberschke, in *X-Ray Absorption Fine Structure,* edited by S. Samar Hasnain (Ellis Horwood, Chichester, England, 1991), p. 193.
[27]T. Yokoyama, T. Satsukawa, and T. Ohta, Jpn. J. Appl. Phys. **28**, 1905 (1989).
[28]H. Rabus, Ph.D. thesis, Freie Universität Berlin, Germany, 1991, p. 120.
[29]D. Arvanitis, T. Lederer, G. Comelli, M. Tischer, T. Yokoyama, L. Tröger, and K. Baberschke, Jpn. J. Appl. Phys. **32**, Suppl. **32-2**, 337 (1993).
[30]A. Frenkel and J. J. Rehr, Phys. Rev. B **48**, 585 (1993).
[31]P. Eisenberger and G. S. Brown, Solid State Commun. **29**, 481 (1979).
[32]E. D. Crozier and A. J. Seary, Can. J. Phys. **58**, 1388 (1980).
[33]E. D. Crozier and A. J. Seary, Can. J. Phys. **59**, 876 (1981).
[34]J. M. Tranquada and R. Ingalls, Phys. Rev. B **28**, 3520 (1983).
[35]J. M. Tranquada, in *EXAFS and Near Edge Structure III,* edited by K. O. Hodpon, B. Hedman, and J. E. Penner-Hahn (Springer, New York, 1984).
[36]E. A. Stern and K. Zhang, Phys. Rev. Lett. **60**, 1872 (1988).
[37]T. Yokoyama, S. Kimoto, and T. Ohta, Jpn. J. Appl. Phys. **28**, L851 (1989); Physica B **158**, 255 (1989); T. Yokoyama and T. Ohta, Jpn. J. Appl. Phys. **29**, 2052 (1990).
[38]H. Maeda, A. Yoshiasa, K. Koto, and T. Ishii, Solid State Ionics **40/41**, 345 (1990).
[39]A. Yoshiasa, H. Maeda, T. Ishii, and K. Koto, Solid State Ionics **40/41**, 341 (1990).
[40]E. A. Stern, P. Livins, and Z. Zhang, Phys. Rev. B **43**, 8850 (1991); E. A. Stern, P. Livins, and Z. Zhang, in *X-Ray Absorption Fine Structure,* edited by S. Samar Hasnain (Ellis Horwood, Chichester, England, 1991), p. 58.
[41]P. Steiner, S. Hüfner, A. Jungmann, V. Kinsinger, and I. Sander, Z. Phys. B **74**, 173 (1989).
[42]G. Bunker, Nucl. Instrum. Methods **207**, 437 (1983).
[43]J. Freund, R. Ingalls, and E. D. Crozier, Phys. Rev. B **39**, 13 537 (1989).
[44]The number of independent parameters which are allowed to be varied in order to fit the experiment is limited (Ref. 45) and care has to be taken not to overinterpret the data (Ref. 46).
[45]P. A. Lee, P. H. Citrin, P. Eisenberger, and B. M. Kincaid, Rev. Mod. Phys. **53**, 769 (1981).
[46]J. Freund, Phys. Lett. A **157**, 256 (1991).
[47]E. A. Stern, D. E. Sayers, and F. W. Lytle, Phys. Rev. B **11**, 4836 (1975).
[48]The minute temperature dependence of $R(T)$ in the EXAFS amplitude of Eq. (2a) is negligible.
[49]J. Freund showed correctly in Ref. 46 that single-shell EXAFS data measured at a fixed temperature could be fitted equally well within the statistical error including and excluding anharmonicity parameters in the fitting routine and concluded that anharmonic information is not present in his data sets. This criticism clearly does not apply to the present analysis: We perform a *comparative* analysis at two different temperatures which greatly reduces the number of free parameters.
[50]For example, Tranquada and Ingalls[34] determined the $\Delta\sigma^2$ term to be -0.008 Å for CuBr between 72 and 295 K, in comparison to the true linear thermal expansion of $\Delta R(295\ \text{K}, 72\ \text{K}) = +0.006$ Å.
[51]E. A. Stern and S. M. Heald, in *Handbook on Synchrotron Radiation,* Vol. 1B, edited by E. E. Koch (North-Holland, New York, 1983), p. 972.
[52]In magnetic resonance: see, for example, I. V. Aleksandrov, *The Theory of Nuclear Magnetic Resonance* (Academic Press, New York, 1966).
[53]G. Beni and P. M. Platzman, Phys. Rev. B **14**, 1514 (1976).
[54]E. Sevillano, M. Meuth, and J. J. Rehr, Phys. Rev. B **20**, 4908 (1979).
[55]M. C. Desjonqueres and G. Treglia, Phys. Rev. B **34**, 6662 (1986).
[56]G. S. Knapp, H. K. Pan, and J. M. Tranquada, Phys. Rev. B **32**, 2006 (1985).
[57]Note that r_0 equals $R(0\ \text{K})$ only in the classical limit.
[58]M. Choi, J. I. Budnick, D. M. Pease, G. H. Hayes, and S. M. Heald, Phys. Rev. B **44**, 9319 (1991).
[59]A. Balerna and S. Mobilio, Phys. Rev. B **34**, 2293 (1986); J. Phys. (Paris) Colloq. **47**, C8-1009 (1986).
[60]W. Böhmer and P. Rabe, J. Phys. C **12**, 2465 (1979).
[61]J. M. Tranquada, S. M. Heald, M. A. Pick, Z. Fisk, and J. L. Smith, J. Phys. (Paris) Colloq. **47**, C8-937 (1986).
[62]G. Dalba, P. Fornasini, F. Rocca, and S. Mobilio, Phys. Rev. B **41**, 9668 (1990).
[63]P. P. Lottici, Phys. Rev. B **35**, 1236 (1987).
[64]S. C. Abrahams and J. L. Bernstein, Acta Cryst. B **25**, 1233 (1969); J. Albertsson, S. C. Abrahams, and Å. Kvick, Acta Cryst. B **45**, 34 (1989).
[65]R. W. G. Wyckoff, *Crystal Structures,* Vol. 1 (Krieger, Malabar, Florida, 1982).
[66]T. Suzuki, J. Phys. Soc. Jpn. **15**, 2018 (1960).
[67]S. Åsbrink and L.-J. Norrby, Acta Cryst. B **26**, 8 (1970).
[68]The maximum k value probed is too short to experience any interference effects between these close lying shells.
[69]M. Choi, J. I. Budnick, D. M. Pease, G. H. Hayes, and J. Wong, in *X-Ray Absorption Fine Structure,* edited by S. Samar Hasnain (Ellis Horwood, Chichester, England, 1991), p. 556.
[70]Y. S. Touloukian, R. K. Kirby, R. E. Taylor, and P. D. Desai, *Thermophysical Properties of Matter,* Vols. 12 and 13 of *Thermal Expansion* (Plenum, New York, 1975).
[71]A k-independent value of 8 Å was used, as the induced errors from this approximation are smaller than 0.003 Å. In all other cases without explicit mention, λ is a k-dependent quantity as calculated from the FEFF code.
[72]Inelastic losses of the photoelectron are incorporated in the FEFF standards through a mean free path [term $\exp(-2R/\lambda)$ in Eq. (2a)].
[73]C. Dagg, L. Tröger, D. Arvanitis, and K. Baberschke, J. Phys. (London) **5**, 6845 (1993); L. Tröger, Ph.D. thesis, Freie Universität Berlin, Germany, 1993.
[74]U. Döbler, K. Baberschke, J. Stöhr, and D. A. Outka, Phys. Rev. B **31**, 2532 (1985).
[75]U. Döbler, K. Baberschke, J. Haase, and A. Puschmann, Phys. Rev. Lett. **52**, 1437 (1984).

[76]M. Bader, A. Puschmann, C. Ocal, and J. Haase, Phys. Rev. Lett. **57**, 3273 (1986).
[77]J. Haase and H.-J. Kuhr, Surf. Sci. **203**, L695 (1988).
[78]J. Stöhr, R. Jaeger, and T. Kendelewicz, Phys. Rev. Lett. **49**, 142 (1982).
[79]K. Baberschke, U. Döbler, L. Wenzel, D. Arvanitis, A. Baratoff, and K. H. Rieder, Phys. Rev. B **33**, 5910 (1986).
[80]L. Wenzel, D. Arvanitis, W. Daum, H. H. Rotermund, J. Stöhr, K. Baberschke, and H. Ibach, Phys. Rev. B **36**, 7689 (1987).
[81]S. R. Chubb, P. M. Marcus, K. Heinz, and K. Müller, Phys. Rev. B **41**, 5417 (1990).
[82]The best notation in the linearized form of the phase shift used in the early days of SEXAFS (approximating the k range of about $k=3-10$ Å^{-1}) is for O-Cu, $\varphi_{\exp}(k)=6.18-0.445$ Å k, and for O-Ni, $\varphi_{\exp}(k)=6.33-0.45$ Å k, where k is defined with respect to the inflection point of the oxygen K edge in the experiment.
[83]W. Oed, H. Lindner, U. Starke, K. Heinz, K. Müller, and J. B. Pendry, Surf. Sci. **224**, 179 (1989).
[84]G. Kleinle, J. Wintterlin, G. Ertl, R. J. Behm, F. Jona, and W. Moritz, Surf. Sci. **225**, 171 (1990).
[85]D. R. Huffman and M. H. Norwood, Phys. Rev. **117**, 709 (1960).
[86]S. S. Todd, J. Am. Chem. Soc. **71**, 4115 (1949).
[87]M. M. Elcombe and A. W. Pryor, J. Phys. C **3**, 492 (1970).
[88]K. Zhang, G. B. Bunker, G. Zhang, Z. X. Zhao, L. Q. Chen, and Y. Z. Huang, Phys. Rev. B **37**, 3375 (1988).
[89]A. N. Mansour, I. Talmy, D. Haught, and R. D. Bardo, in *X-Ray Absorption Fine Structure,* edited by S. Samar Hasnain (Ellis Horwood, Chichester, England, 1991), p. 367.
[90]J. W. Loram, K. A. Mirza, C. P. Joyce, and A. J. Osborne, Europhys. Lett. **8**, 263 (1989).
[91]A. Junod, D. Eckert, G. Triscone, J. Müller, and W. Reichardt, J. Phys. (London) **1**, 8021 (1989).
[92]E. Gmelin, U. Köbler, W. Brill, T. Chattopadhyay, and S. Sastry (unpublished).
[93]W. Schnelle, Diplom thesis, Universität Köln, Germany, 1989.
[94]J. B. Forsyth, P. J. Brown, and B. M. Wanklyn, J. Phys. C **21**, 2917 (1988).
[95]J. H. Broicher, Diplom thesis, Universität Köln, Germany, 1990, p. 55.
[96]*Landolt-Börnstein: Zahlenwerte und Funktionen aus Naturwissenschaft und Technik,* Group III, Vol. 13, part a, edited by K. H. Hellwege and J. L. Olsen (Springer, Berlin, 1981), p. 1.
[97]G. M. Lamble, R. S. Brooks, S. Ferrer, D. A. King, and D. Norman, Phys. Rev. B **34**, 2975 (1986); G. M. Lamble and D. A. King, Philos. Trans. Roy. Soc. London A **318**, 203 (1986).
[98]L. Wenzel, J. Stöhr, D. Arvanitis, and K. Baberschke, Phys. Rev. Lett. **60**, 2327 (1988).
[99]R. Franchy, M. Wuttig, and H. Ibach, Surf. Sci. **203**, 489 (1988).
[100]T. Lederer, D. Arvanitis, G. Comelli, L. Tröger, and K. Baberschke, Phys. Rev. B **48**, 15 390 (1993).
[101]D. R. Warburton, D. Purdie, C. A. Muryn, N. S. Prakash, K. Prabhakaran, G. Thornton, R. A. D. Pattrick, and D. Norman, Phys. Rev. B **45**, 12 043 (1992).
[102]T. Lederer, D. Arvanitis, M. Tischer, L. Tröger, and K. Baberschke, Phys. Rev. B **48**, 11 277 (1993).
[103]J. T. Lewis, A. Lehoczky, and C. V. Briscoe, Phys. Rev. **161**, 877 (1967).
[104]G. Dolling, H. G. Smith, R. M. Nicklow, P. R. Vijayaraghavan, and M. K. Wilkinson, Phys. Rev. **168**, 970 (1968).
[105]M. S. Kushwaha, Nuovo Cimento B **60**, 187 (1980).
[106]Ch. Kittel, *Introduction to Solid State Physics,* 6th ed. (Wiley, New York, 1986), p. 110.
[107]Z. Vardeny, G. Gilat, and D. Moses, Phys. Rev. B **18**, 4487 (1978).
[108]L. Tröger, D. Arvanitis, and K. Baberschke, in *Supraleitung und Tieftemperaturtechnik,* edited by VDI-Technologiezentrum Physikalische Technologien (VDI-Verlag, Düsseldorf, 1993), p. 711.
[109]L. Yang, T. S. Rahman, and D. L. Mills, Phys. Rev. B **42**, 2864 (1990).

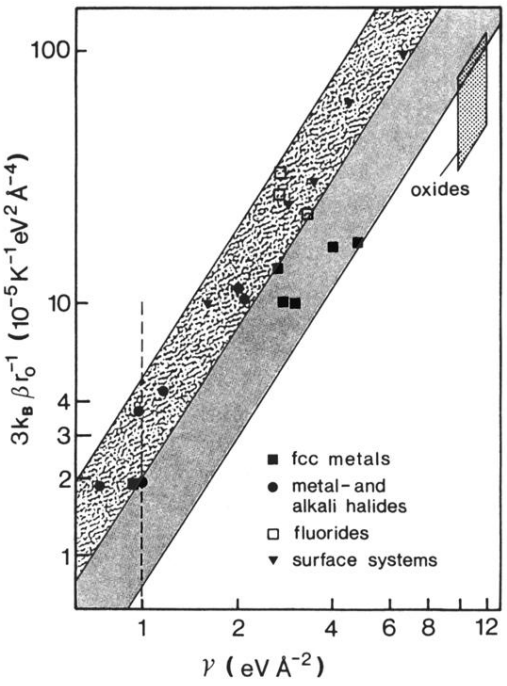

FIG. 7. Double logarithmic correlation diagram of γ versus $3k_B\beta/r_0$. γ and β are the harmonic force constant and the anharmonicity constant of the anharmonic pair interaction potential [Eq. (7)] between absorbing and backscattering atom. The upper (textured) and lower (grey) regions mark different high-temperature saturation values of the coefficient of linear thermal expansion of above and below 2×10^{-5} K^{-1} which can be read from the $\gamma=1$ eV Å^{-2} intercept (dashed line). Within the dotted area bulk oxides are located. See text for further discussion.